PHYSICAL REVIEW B **87**, 121404(R) (2013)

Measurement of layer breathing mode vibrations in few-layer graphene

Chun Hung Lui and Tony F. Heinz*

Departments of Physics and Electrical Engineering, Columbia University, 538 West 120th Street, New York, New York 10027, USA

(Received 1 December 2012; published 12 March 2013)

Layer-layer coupling plays a critical role in defining the physical properties of few-layer graphene. With respect to vibrations, for each layer thickness N, interlayer coupling creates a set of $N-1$ out-of-plane layer breathing modes (ZO′) with finite frequencies at the zone center. Unlike the widely studied intralayer vibrations, the properties of these layer breathing modes (LBMs) are defined by the layer-layer interactions. Here we report the observation of distinct LBMs for Bernal stacked graphene of layer thicknesses $N = 2$–20 through measurement of electronically resonant overtone Raman bands. The Raman bands exhibit multipeak features that are unique for graphene samples of each layer thickness. The frequencies can be described well using a simple linear-chain model based on nearest-neighbor couplings between the layers.

DOI: 10.1103/PhysRevB.87.121404 PACS number(s): 78.67.Wj, 78.30.−j, 73.22.Pr

Mono- and few-layer graphene (FLG) are attractive materials because of their distinctive physical properties and their potential for novel applications.[1–3] A striking feature of FLG is that each layer thickness possesses a unique low-energy electronic structure, with interlayer coupling yielding a rich spectrum of electronic properties for the materials.[1–9] Similar distinctive features are also predicted with regard to phonons, with a set of different low-energy *interlayer* vibrational modes associated with each layer thickness. The interlayer vibrations comprise shearing modes[10] and layer breathing modes[11–17] [LBMs or ZO′, Fig. 1(a)]. These vibrations involve, respectively, the relative displacement of the individual graphene layers in the tangential and perpendicular directions. The LBMs are of great scientific and practical significance because their out-of-plane layer displacements render them highly sensitive to interaction between the graphene layers. Although the LBM was studied in bulk graphite,[18,19] multiwalled carbon nanotubes,[20,21] and also explored theoretically in FLG,[11–17] experimental study of the LBM has proven to be challenging because of the low frequency of the vibrations and the atomic-level thinness of the samples. Previous studies have reported experimental signatures of LBMs in FLG through Raman spectroscopy of LO + ZO′ combination modes.[22–24] Detailed study of the low-frequency LBMs through this approach has, however, been impeded by the much larger vibrational frequency of the in-plane longitudinal optical (LO) phonon involved in the combination mode, which makes precise extraction of the frequencies of the LBMs difficult. A recent investigation[25] of FLG grown by chemical vapor deposition reported observation of a single LBM by Raman and coherent phonon spectroscopy, but detailed information on the different LBMs in FLG and their evolution with layer thickness is still lacking.

In this Rapid Communication, we report a comprehensive determination of the different LBM frequencies for FLG by means of the two-phonon overtone spectra observed in doubly resonant Raman spectroscopy. For FLG from two to 20 layers over the spectral range of 80–300 cm^{-1}, we find features arising from *each of the different LBM vibrations*. These numerous 2ZO′ Raman features shift systematically as the layer thickness of graphene increases. The behavior reflects the increasing number and the shifting frequencies of the different ZO′ normal modes in thicker graphene layers. We show that these frequencies can be described surprisingly accurately using a simple model based on nearest-neighbor couplings between the layers, equivalent to a one-dimensional chain of N coupled masses. Our research of the LBMs extends the previous Raman studies on another interlayer mode, namely, the shearing mode in FLG (Ref. 10) and two-dimensional transition metal dichalcogenides.[26]

We investigated pristine free-standing graphene layers prepared by mechanical exfoliation of kish graphite (Covalent Materials Corp.). The free-standing graphene samples were deposited on quartz substrates with prepatterned trenches (4 μm width and 0.5 μm depth). We examined graphene with thicknesses from single layer up to 20 layers, all with Bernal stacking order. The layer thickness and stacking order were characterized by several methods, including infrared spectroscopy,[9,27,28] optical contrast measurements in the visible range, Raman spectroscopy of the 2D[29–32] and the LOZO′ combination mode,[22,24] and atomic force microscopy (AFM). In particular, infrared conductivity measurements, although only having been studied in detail for FLG up to eight layers,[9] were found to be valuable for analysis of still thicker films. For the thickest films investigated, tentative assignments of the layer number were confirmed by the smooth evolution of LBM spectra reported here.

The Raman measurements were performed using a commercial confocal microRaman system (JY-Horiba labRAM ARAMIS) equipped with a cooled charge-coupled device (CCD) array detector and purged with argon. Laser excitation sources were available with photon energies (wavelengths) of $E_{exc} = 1.58$ eV (785 nm), 1.96 eV (633 nm), and 2.33 eV (532 nm). The laser power was consistently maintained below 5 mW, with a spot size of a few microns on the sample. As heat dissipation is reduced for suspended graphene, we observed some heating effect in our samples. This was estimated to cause a redshift of ~ 2 cm^{-1} for the 2ZO′ Raman peak, but had little effect on the line shape of all measured Raman spectra. In addition, no significant changes in the 2ZO′ features were found in repeated measurements of different FLG samples of the same thickness, indicating the robustness of the results against variation in sample conditions, such as unintentional doping and strain.

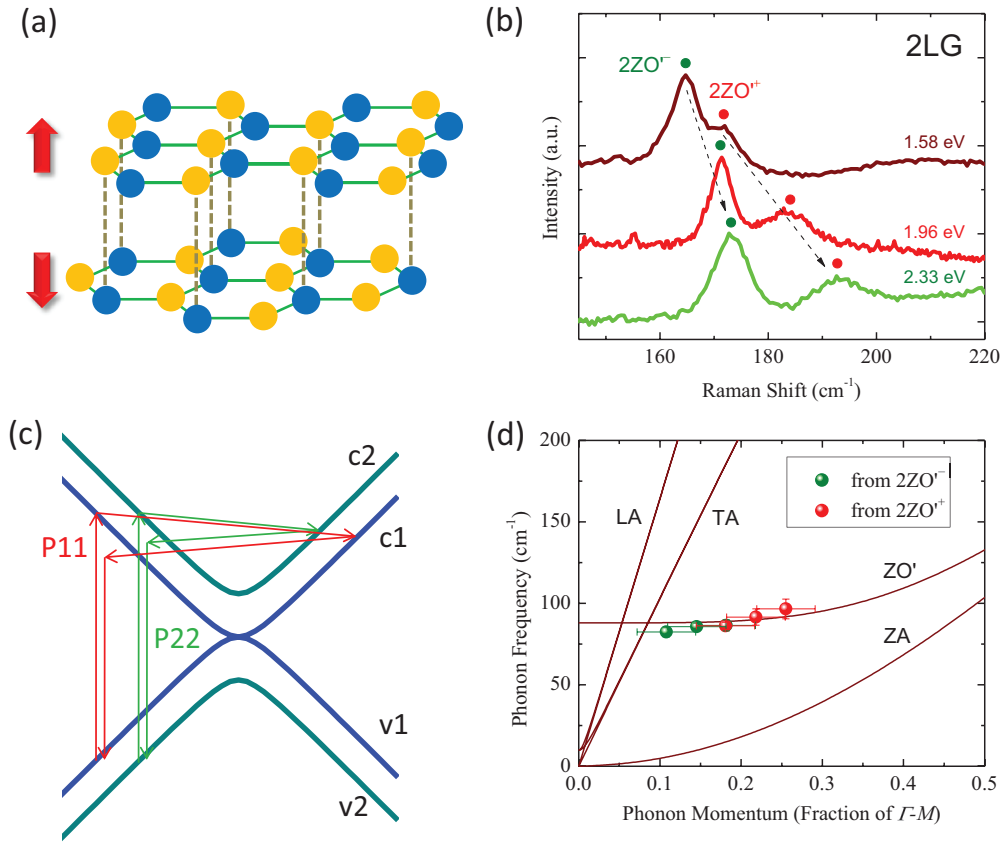

FIG. 1. (Color online) The layer breathing mode for bilayer graphene. (a) Schematic representation of the atomic displacement for the LBM in 2LG. (b) Normalized 2ZO′-mode spectra of 2LG at different laser excitation energies E_{exc}. The high- and low-energy components of the 2ZO′ band are denoted as $2ZO'^{+}$ and $2ZO'^{-}$, respectively. (c) The main electronic scattering processes in the two-phonon double-resonance Raman mechanism of the 2ZO′ mode in 2LG. (d) The ZO′-mode phonon dispersion (symbols) extracted from (b). The phonon frequency is obtained as half of the value of the Raman shift for the peaks in (b) through fits by a double Gaussian function. The error bars reflect the widths of the Gaussian fit functions. The $2ZO'^{+}$ and $2ZO'^{-}$ peaks are ascribed to the P11 and P22 processes in (c), respectively. The corresponding error bars represent uncertainties in estimating the phonon momenta in these scattering processes. The experimental data are compared with the theoretically predicted dispersion (Ref. 16) for the LBM in 2LG (lines).

Let us first consider the Raman response of bilayer graphene (2LG). This material should exhibit only a single LBM, corresponding to the symmetric oscillation of the two sheets of graphene about the center of the structure [Fig. 1(a)]. Over a frequency range of 145–220 cm^{-1}, we observed a double-peak feature at ∼180 cm^{-1} [Fig 1(b)]. Although the intensity of this feature is approximately 100 times weaker than that of the G-mode response of the intraplane vibrations, these low-frequency peaks are clearly observable. However, no corresponding Raman feature is observable for single-layer graphene, as expected for a response arising from interlayer vibrations. As the laser photon energy E_{exc} increases from 1.58 to 2.33 eV, the Raman band of 2LG significantly blueshifts. The line shape also changes, with the two components separating more widely from one another.

This strongly dispersive Raman response indicates that we are observing a higher-order Raman process, like the 2D mode, which is known to be highly efficient for graphitic materials through mechanisms involving electronic resonances.[29–31,33,34] We have analyzed the dispersion behavior of the measured 2LG Raman response using double-resonance theory. We assign the features to the overtone (2ZO′) mode of the layer breathing vibration [Fig. 1(a)] occurring through an intravalley resonance processes. In our treatment, we have adopted the electronic band structure of 2LG within a simplified tight-binding (TB) model that includes just the dominant intra- (γ_0) and interlayer (γ_1) couplings. (We note, however, that analysis using more accurate band structure does not significantly modify the results.) 2LG has two conduction (valence) bands, $c1$ and $c2$ ($v1$ and $v2$), which give rise to four possible electronically resonant processes (P11, P22, P12, and P21) for the intravalley two-phonon scattering [Fig. 1(c)]. Group theory[35] shows that P12 and P21 are forbidden at the high-symmetry points along the Γ-M and M–K lines in the Brillouin zone (BZ) of 2LG, thus suppressing these processes. We can then assign the high- and low-energy component peaks ($2ZO'^{+}$ and $2ZO'^{-}$) of the observed Raman feature, respectively, to the P11 and P22 processes.

With the aid of these assignments we can estimate the dominant phonon momenta in the resonant Raman processes for different values of E_{exc}. Figure 2(d) displays the phonon energies, obtained as half of the values of the $2ZO'^{+}$ and $2ZO'^{-}$ peaks, as a function of the phonon momentum. We

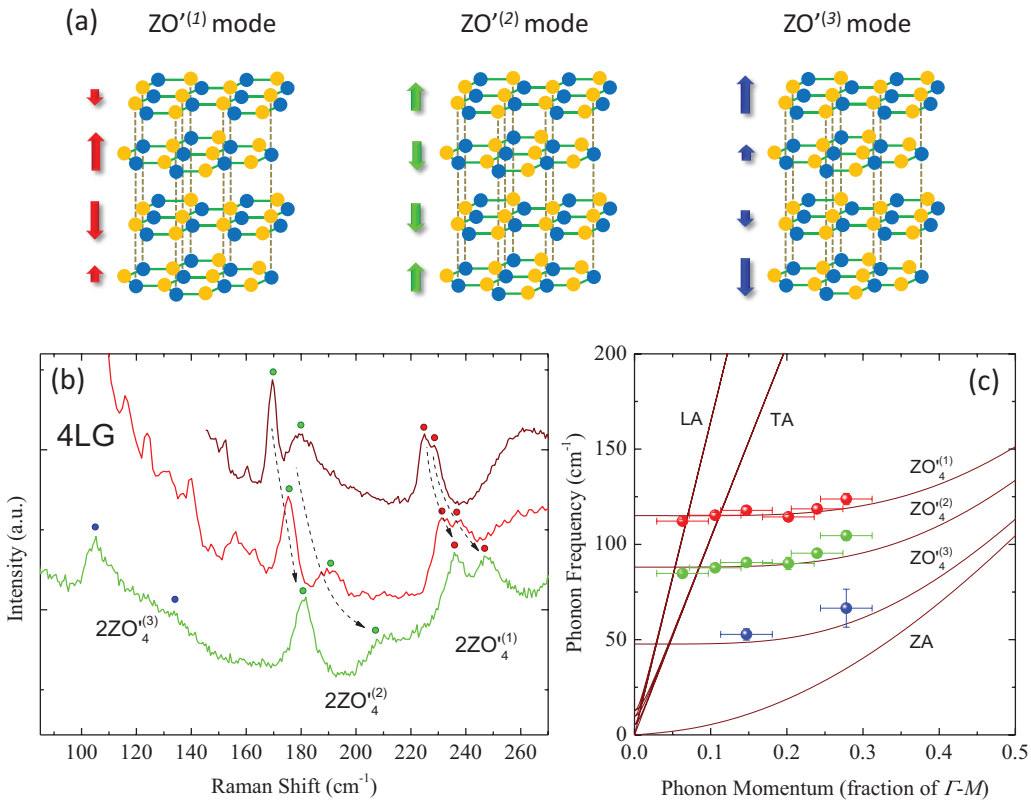

FIG. 2. (Color online) The layer breathing modes for 4LG. (a) Schematic representation of the atomic displacements for the three ZO′ modes in 4LG. The length of the arrows represents the magnitude of the vibration. (b) Raman spectra of the three 2ZO′ modes in 4LG for $E_{\text{exc}} = 1.58$ (upper trace), 1.96 (middle trace), and 2.33 eV (lower trace). (c) ZO′-mode phonon dispersion, extracted from (b). In determining the phonon momenta, we assume that the high- (low)-frequency components of the overtone modes arise from electronic processes with the maximum (minimum) phonon wave vector defined by the band structure of 4LG for the double-resonance Raman scattering. The experimental data are compared with the theoretically predicted dispersion (Ref. 16) of the low-frequency phonon modes in 4LG.

compare the experimental results with the predicted dispersion relation for the ZO′ mode in 2LG.[16] The good agreement between experiment and theory confirms our assignment of the 2ZO′ overtone mode. From the results we can extrapolate the ZO′-mode frequency for 2LG at the Γ point to be 80 ± 2 cm^{-1}, a result comparable to theoretical predictions.[12,16] This latter frequency corresponds to that of oscillation in the relative displacement of two *rigid* graphene sheets in the bilayer. The only other interlayer mode present for 2LG is the shearing mode.[10] For the range of wave vectors relevant in the double-resonance process, it is, however, expected to lie at a considerably higher frequency [transverse acoustic (TA) and longitudinal acoustic (LA) branches in Fig. 1(d)].

We now extend our discussion to the behavior of thicker samples of FLG. As additional layers of graphene are added beyond the bilayer, new normal modes develop. For N-layer graphene (NLG), the interlayer coupling will create $N-1$ distinct ZO′ branches (with finite frequencies at the zone center). We denote these modes as $\text{ZO}'^{(n)}_N$ [or simply as $\text{ZO}'^{(n)}$ if N is clear from the context], where the index $n = 1,2,\ldots,N-1$ represents the branch number, enumerating from high- to low-mode frequency. The highest-frequency mode will correspond to alternating displacements of adjacent graphene planes, while lower-frequency modes will involve more layers moving in the same direction and experiencing consequently a weaker overall restoring force. Remarkably, as we show below, we are able to *observe all of these different LBMs* within our experimental spectral range for samples up to 20 layers in thickness.

As an illustration of the evolution of behavior with increasing layer thickness, we consider 4LG. 4LG possesses three relevant ZO′ branches, $\text{ZO}'^{(1)}_4$, $\text{ZO}'^{(2)}_4$, and $\text{ZO}'^{(3)}_4$, the layer displacements of which are shown schematically in Fig. 2(a). In accordance, we observe three Raman features in the spectral range of 85–270 cm^{-1} for $E_{\text{exc}} = 2.33$ eV [Fig. 2(b)]. Each feature shows a double peak, with positions and line shapes that evolve with E_{exc} in a manner similar to those of the 2ZO′ mode in 2LG. To confirm the origin of these Raman bands, we adopt the same analysis for the 2LG case, but using a 4LG TB electronic structure, again derived including only the dominant couplings γ_0 and γ_1. Since the 4LG electronic structure exhibits four conduction (valence) bands, the electronic processes for intravalley two-phonon resonant Raman scatterings are numerous and complex. For simplicity, we assume that the high- and low-frequency components of the double-peaked Raman features arise from electronic processes with the maximum and minimum phonon momentum, respectively. We then obtain the phonon frequencies as a function of momentum [Fig. 2(c)]. We find that the experimental results match well with the theoretical dispersion[16] of the $\text{ZO}'^{(1)}_4$,

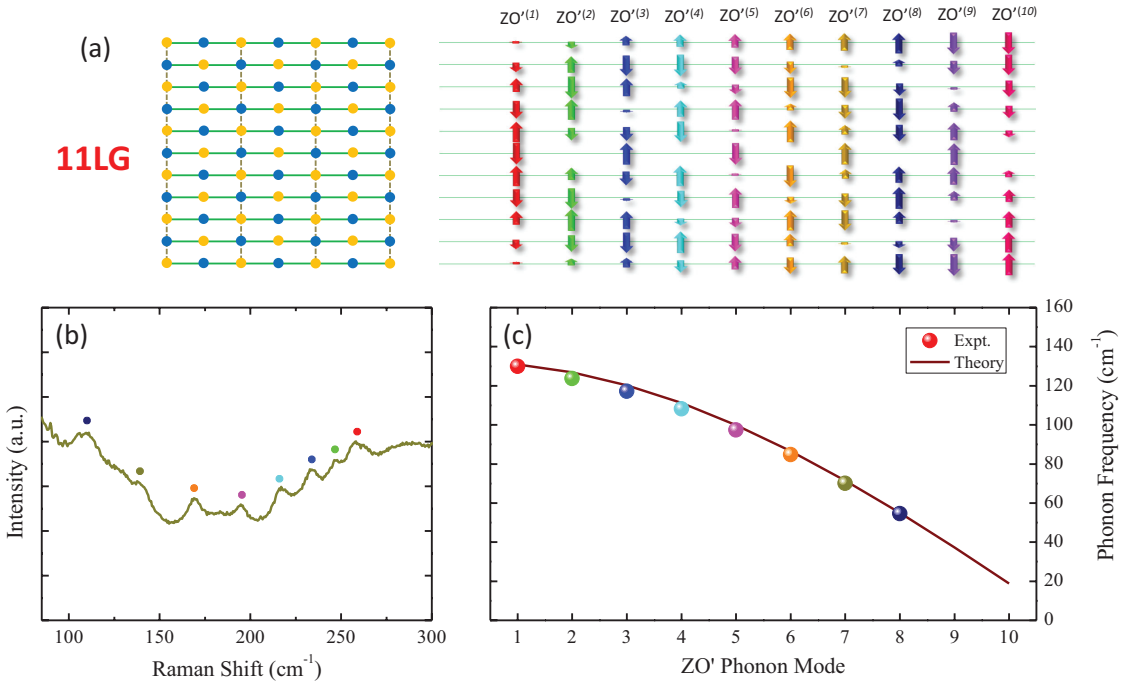

FIG. 3. (Color online) The layer breathing modes for 11LG. (a) Schematic representation of the atomic displacements of the ten different ZO′ modes in 11LG. The left panel shows the layer structure of 11LG sample. The right panel shows the layer displacement in each ZO′ mode, with arrows drawn in proportion to magnitude of the displacement. (b) The 2ZO′-mode Raman spectrum of 11LG for $E_{\text{exc}} = 2.33$ eV. (c) The ZO′-mode phonon frequency, obtained as half of the frequency of the corresponding overtone Raman peaks in (b). The experimental data are compared with the predictions of the model described in the text [Eq. (1)] for the ZO′-mode frequencies of 11LG.

$ZO_4'^{(2)}$, and $ZO_4'^{(3)}$ phonon modes. Similar results hold for analysis on 3LG.

For graphene samples of still greater thickness, we observe the emergence of new Raman features, corresponding to the presence of additional LBMs. For 11LG [Figs. 3(a)–3(c)], for example, we have ten LBMs, $ZO_{11}'^{(1)}$–$ZO_{11}'^{(10)}$. We observe eight distinct Raman peaks in the spectral range of 85–300 cm^{-1} for $E_{\text{exc}} = 2.33$ eV. As we show below by quantitative analysis, we can identify these features with overtones of the $ZO_{11}'^{(1)}$–$ZO_{11}'^{(8)}$ phonon branches [Fig. 3(c)]. The two lowest-frequency phonon modes, $ZO_{11}'^{(9)}$ and $ZO_{11}'^{(10)}$, are not present because of the restricted spectral range of observation.

We have examined the Raman spectra of suspended graphene samples with each thickness $N = 2,3,4,\ldots,20$, as well as bulk graphite, all with Bernal stacking. In the frequency range of 80–300 cm^{-1}, we find a panoply of Raman peaks. The observed frequencies and line shapes are unique for graphene of each layer thickness [Fig. 4(a)]. With increasing layer thickness, the number of 2ZO′ Raman peaks grows systematically and the spectral shape of the whole band gradually approaches that of the graphite spectrum. The above observations highlight the remarkable sensitivity of the LBMs to interlayer interactions. In particular, the 2ZO′ peaks are still distinct for 20LG, indicating that they can be used as an accurate spectroscopic signature to characterize, with atomic level precision, the layer thickness of graphene up to 20 layers.

We now show that the frequencies of the different LBM vibrations can be described well by a remarkably simple model, namely, one in which all layers are treated as equivalent and only nearest-neighbor interactions between the layers are considered. Within this picture, the various LBM modes $ZO_N'^{(n)}$ are equivalent to the normal vibration modes of a linear chain of N masses connected by springs. The solution to this classic problem[36] yields mode frequencies of

$$\omega_N(n) = \omega_o \sin[(N-n)\pi/2N], \tag{1}$$

where ω_o denotes the frequency of the bulk optical mode or, equivalently, $\omega_o/\sqrt{2}$ corresponds to the frequency of the LBM in the bilayer. To adapt this simple analysis to our problem, we chose $\omega_o = 132.3$ cm^{-1} as the ZO′ mode frequency observed in bulk graphite, as obtained from the measured frequency of the 2ZO′ Raman peak (264.5 cm^{-1}) [Fig. 4(a)]. As the 2ZO′ mode involves phonons of finite momentum selected through the double-resonance Raman process, a minor error (~2 cm^{-1}) is expected from the in-plane phonon dispersion of the LBMs near the zone center. The results of Eq. (1) provide an excellent overall fit to the experimental data for all layer thicknesses [Fig. 4(b)]. The results for 11LG [Fig. 3(c)] highlight the good agreement that is achieved. The modest observed deviations presumably reflect the approximate treatment of the finite in-plane wave vector in the data, as well as limitations in the model, such as its assumption that the interactions between graphene layers are identical, irrespective of layer thickness or position. Since suspended graphene samples were investigated, we expect that perturbations of the external environment will be negligible.

For further analysis on the LBMs in FLG, we observe that, within a model of nearest-layer interactions, the frequencies

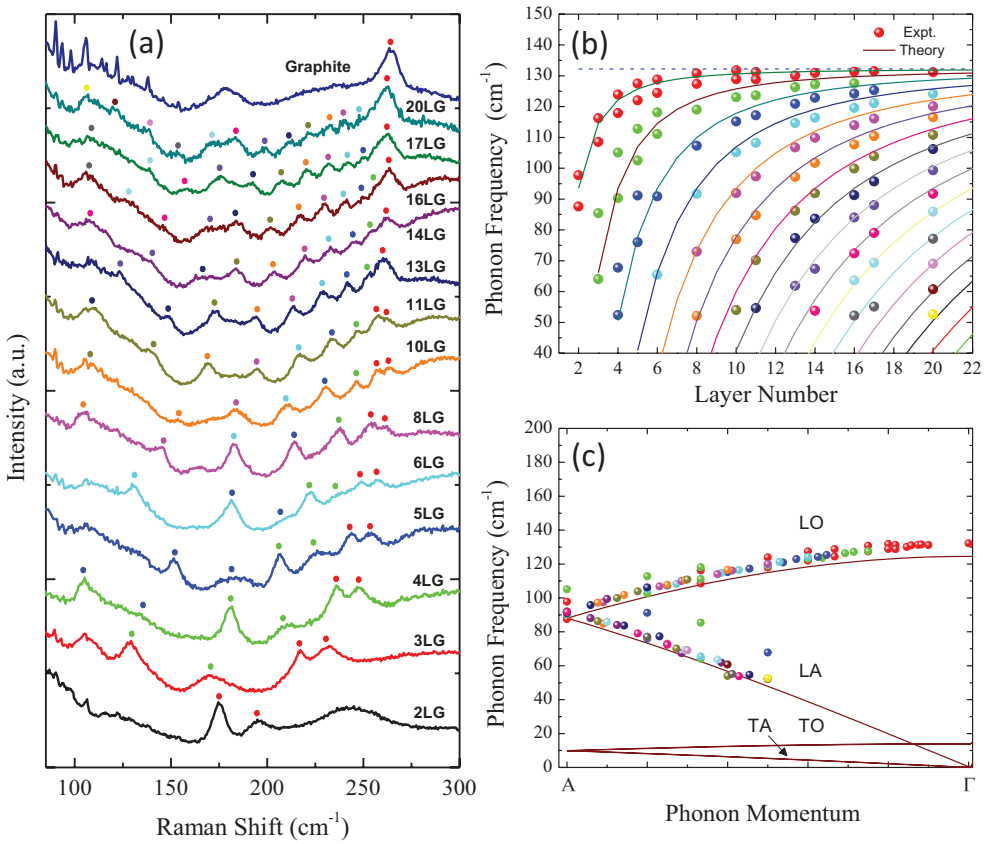

FIG. 4. (Color online) The layer breathing modes for FLG. (a) The 2ZO′-mode Raman spectra for FLG with $N = 2$ to 20 and for the bulk graphite. The spectra are shifted for clarity. (The sharp features below 150 cm^{-1} in the graphite spectrum arise from the Raman scattering of air. The spikes are more visible in graphite than in FLG because of the reflection of the laser from the graphite surface.) (b) The ZO′-mode phonon frequencies, obtained from the overtone Raman peaks in (a), as a function of layer thickness. The experimental results (symbols) are compared with theory (lines) as described in the text [Eq. (1)]. The dashed line denotes the ZO′-mode frequency measured in bulk graphite. (c) The LBM phonon dispersion along the A-Γ line in graphite, constructed from the data in (b) within a zone-folding scheme, in comparison with the theoretically predicted dispersion (Ref. 16) of the low-frequency phonons in graphite.

of the various $ZO'^{(n)}_N$ modes are the same as the frequencies of the bulk graphite ZO′ mode for out-of-plane wave vectors of $(\pi/c)(N-n)/N$ along the Γ-A line in the three-dimensional graphite Brillouin zone, where $c \approx 0.34$ nm is the interlayer spacing. We have applied this scheme to reconstruct the expected graphite phonon dispersion along the Γ-A line using the observed 2ZO′ modes in FLG [Fig. 4(c)]. We find good overall agreement between experiment and existing calculations.[16] The experimental results appear to be slightly higher than the theoretical values as expected because of the finite in-plane phonon dispersion of the LBMs selected in the doubly resonant Raman measurements.

As can be seen in Figs. 4(a) and 4(b), multiple subpeaks (denoted by dots of the same color) are observed for some 2ZO′ Raman features. They are associated with the same $ZO'^{(n)}_N$ branch, but for phonons of different momenta, in agreement with our earlier analysis of the double-resonance effects on the 2LG and 4LG spectra. Although it is difficult to analyze fully the complex underlying resonant processes, here we comment on some key characteristics of these multipeaked Raman features. First, the $2ZO'^{(n)}_N$ peaks generally exhibit just two components. This implies that, although the electronic bands in FLG are numerous, they give rise to resonant Raman processes involving only a small number of dominant phonon momenta. Second, the separation between the two components decreases with increasing layer number N and decreasing branch index n. This trend can be understood by the fact that the $ZO'^{(n)}_N$ branches become less dispersive near the zone center. The higher the Γ-point ZO′-mode frequency is, the flatter is the corresponding phonon branch. Since the ZO′-mode frequency at the Γ point increases with increasing N or decreasing n, this leads to weaker dispersion of the $ZO'^{(n)}_N$ branch, and, hence, smaller separations between the $ZO'^{(n)}_N$ components. Third, the high-frequency $ZO'^{(n)}_N$ components tend to be weaker and broader than the low-frequency ones. We may understand this observation by considering the increasingly stronger dispersion of the ZO′ phonons at greater distances from the Γ point. In the double-resonance Raman process, a larger Raman shift implies larger wave vectors for the corresponding ZO′ phonon. The larger dispersion of such ZO′ phonons is then expected to produce a broader feature in the corresponding Raman spectrum. Fourth, the high-frequency components deviate significantly from the theoretical predictions [Figs. 4(b) and 4(c)]. We take this as

an indication of the important role of the selection of the in-plane wave vector in the electronically resonant Raman process.[37]

Finally, we comment on the possibility of combination modes of ZO′ phonons from different branches occurring in our observed Raman spectra. Let us first consider the graphite spectrum [Fig. 4(a)], which exhibits two prominent peaks at 180 and 265 cm^{-1}. The latter can be readily interpreted as the 2ZO′ overtone band arising from a singularity of the LBM phonon density of state (DOS) at the Γ point [Fig. 4(c)]. The former, however, cannot be explained in this way due to the lack of similar singularity in this energy range. This leads us to consider two-phonon combination modes. Since the two scattered phonons must have equal (but opposite) momentum in the out-of-plane (Γ-*A*) direction, the only allowed combinations are of one LO- and one LA-branch LBM phonon with the same momentum [Fig. 4(c)]. The resultant LO + LA combination modes will involve frequencies close to the double value of the *A*-point LBM phonon frequency, where a singularity in the two-phonon DOS occurs. This accounts naturally for the Raman peak at 180 cm^{-1} in graphite. The above selection rules should still be approximately valid for FLG. Correspondingly, we would expect a significant Raman response only from $ZO_N'^{(n)} + ZO_N'^{(N-n)}$ combination modes, which would satisfy the condition of vanishing total phonon momentum in the bulk limit. Such combination modes are limited to a spectral range around 150–200 cm^{-1}. In this region, we do see somewhat enhanced Raman peaks, possibly arising from a contribution of these combination modes in addition to the dominant overtone response [Fig. 4(a)]. Such propensity rules for the combination modes are supported by the complete absence of any peaks in the experimental Raman spectra at frequencies not compatible with an overtone mode, such as what would occur for a $ZO_N'^{(n)} + ZO_N'^{(n+1)}$ combination mode.

In conclusion, our study has shown the evolution of interlayer breathing vibrational modes of few-layer graphene from bilayer to the bulk limit. For each layer thickness, we observe a whole family of distinct layer breathing modes. The seemingly complex and layer-dependent behavior of layer breathing modes can be described well within a model based on nearest-neighbor couplings between the layers. In addition to providing a direct probe of the interlayer interactions and low-energy phonons in few-layer graphene, our research also demonstrates an accurate optical technique for the determination of layer thickness. Measurement of the LBM Raman spectrum presented here complements the well-established approach of Raman analysis using the 2D mode[30,31] by extending the range of thickness up to 20 layers. The method described in this Rapid Communication also opens up the possibility for investigation of the role of adsorbates and the surrounding media on the characteristics of the LBM vibrations.

We thank K. Knox, S. H. Kim, and D. Q. Zhang for their assistance in sample and substrate preparation, L. M. Malard for discussions, and L. J. Karssemeijer and A. Fasolino for sharing their theoretical calculation of the low-energy phonon dispersion of FLG and graphite. We acknowledge support from the Office of Naval Research under the MURI program and from Department of Energy, Basic Energy Sciences under Grant No. FG02-07ER15842.

*Author to whom correspondence should be addressed: tony.heinz@columbia.edu

[1] A. K. Geim, Science **324**, 1530 (2009).
[2] A. H. Castro Neto, F. Guinea, N. M. R. Peres, K. S. Novoselov, and A. K. Geim, Rev. Mod. Phys. **81**, 109 (2009).
[3] S. Das Sarma, S. Adam, E. H. Hwang, and E. Rossi, Rev. Mod. Phys. **83**, 407 (2011).
[4] F. Guinea, A. H. C. Neto, and N. M. R. Peres, Phys. Rev. B **73**, 245426 (2006).
[5] S. Latil and L. Henrard, Phys. Rev. Lett. **97**, 036803 (2006).
[6] B. Partoens and F. M. Peeters, Phys. Rev. B **74**, 075404 (2006).
[7] M. Koshino and T. Ando, Phys. Rev. B **76**, 085425 (2007).
[8] H. K. Min and A. H. MacDonald, Prog. Theor. Phys. Suppl. **176**, 227 (2008).
[9] K. F. Mak, M. Y. Sfeir, J. A. Misewich, and T. F. Heinz, Proc. Natl. Acad. Sci. USA **107**, 14999 (2010).
[10] P. H. Tan *et al.*, Nat. Mater. **11**, 294 (2012).
[11] S. Kitipornchai, X. Q. He, and K. M. Liew, Phys. Rev. B **72**, 075443 (2005).
[12] S. K. Saha, U. V. Waghmare, H. R. Krishnamurthy, and A. K. Sood, Phys. Rev. B **78**, 165421 (2008).
[13] J.-W. Jiang, H. Tang, B.-S. Wang, and Z.-B. Su, Phys. Rev. B **77**, 235421 (2008).
[14] K. H. Michel and B. Verberck, Phys. Rev. B **78**, 085424 (2008).
[15] H. Wang, Y. F. Wang, X. W. Cao, M. Feng, and G. X. Lan, J. Raman Spectrosc. **40**, 1791 (2009).
[16] L. J. Karssemeijer and A. Fasolino, Surf. Sci. **605**, 1611 (2011) and private communication.
[17] K. H. Michel and B. Verberck, Phys. Rev. B **85**, 094303 (2012).
[18] R. Nicklow, N. Wakabayashi, and H. G. Smith, Phys. Rev. B **5**, 4951 (1972).
[19] M. Mohr *et al.*, Phys. Rev. B **76**, 035439 (2007).
[20] C. Spudat *et al.*, Nano Lett. **10**, 4470 (2010).
[21] D. Levshov *et al.*, Nano Lett. **11**, 4800 (2011).
[22] F. Herziger, P. May, and J. Maultzsch, Phys. Rev. B **85**, 235447 (2012).
[23] K. Sato *et al.*, Phys. Rev. B **84**, 035419 (2011).
[24] C. H. Lui *et al.*, Nano Lett. **12**, 5539 (2012).
[25] J. Shang *et al.*, J. Raman Spectrosc. **44**, 70 (2013).
[26] G. Plechinger *et al.*, Appl. Phys. Lett. **101**, 101906 (2012).
[27] K. F. Mak, J. Shan, and T. F. Heinz, Phys. Rev. Lett. **104**, 176404 (2010).
[28] C. H. Lui, Z. Li, K. F. Mak, E. Cappelluti, and T. F. Heinz, Nat. Phys. **7**, 944 (2011).
[29] A. C. Ferrari *et al.*, Phys. Rev. Lett. **97**, 187401 (2006).
[30] A. C. Ferrari, Solid State Commun. **143**, 47 (2007).
[31] L. M. Malard, M. A. Pimenta, G. Dresselhaus, and M. S. Dresselhaus, Phys. Rep. **473**, 51 (2009).

[32]C. H. Lui *et al*., Nano Lett. **11**, 164 (2010).
[33]C. Thomsen and S. Reich, Phys. Rev. Lett. **85**, 5214 (2000).
[34]R. Saito *et al*., Phys. Rev. Lett. **88**, 027401 (2001).
[35]L. M. Malard, M. H. D. Guimaraes, D. L. Mafra, M. S. C. Mazzoni, and A. Jorio, Phys. Rev. B **79**, 125426 (2009).
[36]S. T. Thornton and J. B. Marion, *Classical Dynamics of Particles and Systems*. (Brooks Cole, Pacific Grove, CA, 2003).
[37]See Supplemental Material at http://link.aps.org/supplemental/10.1103/PhysRevB.87.121404 for a comparative study of the 2ZO′ mode of *ABA* and *ABC* stacked 3LG that illustrates the influence of the FLG electronic structure on the LBM Raman spectrum.